Journal of Membrane Science 578 (2019) 136–148

Contents lists available at ScienceDirect

Journal of Membrane Science

journal homepage: www.elsevier.com/locate/memsci

Chemically stabilised extruded and recast short side chain Aquivion® proton exchange membranes for high current density operation in water electrolysis

Stefania Siracusano[a], Claudio Oldani[b], Maria Assunta Navarra[c], Stefano Tonella[b], Lucia Mazzapioda[c], Nicola Briguglio[a], Antonino S. Aricò[a,*]

[a] CNR-ITAE Institute of Advanced Energy Technologies, National Research Council, Via Salita S. Lucia Sopra Contesse 5, 98126 Messina, Italy
[b] Solvay Specialty Polymers Italy S.p.A., Viale Lombardia 20, 20021 Bollate Mi, Italy
[c] Department of Chemistry, University of Rome "La Sapienza", P.le Aldo Moro 5, 00185 Roma, Italy

ARTICLE INFO

Keywords:
Electrolysis
Polymer electrolyte membrane
Hydrogen
Extruded membrane
Recast membrane

ABSTRACT

Membrane-electrode assemblies based on chemically stabilised short-side-chain proton exchange Aquivion® membranes, prepared by extrusion or recast methods, have been investigated for operation at high current density (3–4 A cm^{-2}) in water electrolysis cells. A thickness of 90 μm was selected for these perfluorosulfonic acid membranes in order to provide proper resilience to hydrogen crossover under differential pressure operation while allowing operation at high currents. The membranes showed proper mechanical strength for high-pressure operation and suitable conductivity to reduce ohmic losses at high current densities. Both membranes showed excellent performance in electrolysis cells by achieving a voltage efficiency better than 85% and 80% (1.85 V) at 3 and 4 A cm^{-2}, respectively, in polarisation curves at 90 °C. A smaller surface roughness was observed from atomic force microscopy for the recast membrane compared to the extruded one. This may affect the intimate contact between the ionic clusters of the membrane and the catalyst agglomerate at the interface producing a catalytic enhancement in the activation region of the polarisation curves in the case of the recast membrane. At high cell voltages, the polarisation resistance was instead slightly lower for the cell based on the extruded membrane. Interestingly, the different characteristics of the membrane-electrodes interface produced lower recoverable losses in durability studies for the recast membrane-based electrolyser allowing stable operation at both 3 and 4 A cm^{-2}. Hydrogen crossover analysis at a differential pressure of 20 bar showed low gas permeation through both membranes allowing for a wide load range (15–100%) and high faradaic efficiency > 99% at practical current densities (1–4 A cm^{-2}).

1. Introduction

Energy storage in hydrogen is a promising technology for the next generation energy system being both scalable and geographically independent [1,2]. Hydrogen as fuel is characterised by high gravimetric energy density and clean combustion [3,4]. It is expected that a wide use of this energy vector will assume in the future an increased environmental and societal relevance especially in providing a solution for the energy issues while mitigating pollution, global warming and related effects of climate changes [5–7].

One of the most advanced processes to produce highly pure "green" hydrogen from renewable energy is based on the polymer electrolyte membrane (PEM) water electrolysis [8,9]. PEM water electrolysers operate at high pressure to reduce down-stream gas compression thus allowing efficient hydrogen storage [10–13]. A key aspect of this technology is its excellent dynamic behaviour for proper interfacing with intermittent renewable power sources and its suitable application in grid-balancing service [1,9,14]. However, the cost of the hydrogen produced from PEM electrolysis is still high compared to competitive technologies like central steam reforming of natural gas [8,9].

Despite the increasing concerns raised by the effects of greenhouse gases emissions and the related global warming, the transition towards sustainable energy technologies is slowed by a low economic competitiveness [15]. In the next future, a larger diffusion of renewable energy sources will necessarily cause an increase of the surplus of energy associated to their intermittent behaviour [16]. This may produce very likely a decrease of the electricity cost in specific periods. Moreover, a significant fraction of energy is expected to be curtailed by the grid operators when the demand from the customers will be low. Accordingly, a cost-effective and dynamic energy conversion/storage system,

* Corresponding author.
E-mail address: arico@itae.cnr.it (A.S. Aricò).

https://doi.org/10.1016/j.memsci.2019.02.021
Received 2 January 2019; Received in revised form 6 February 2019; Accepted 10 February 2019
Available online 14 February 2019
0376-7388/

operating on a wide scale, can provide an effective solution to enhance the utilisation of the produced renewable energy while avoiding significant implementation of the electricity grid infrastructure [9].

To allow for a widespread utilisation of the PEM electrolysis technology, a significant reduction of the capital costs is strongly necessary [9]. This will make the hydrogen produced from electrolysis competitive with respect to the currently used organic fuels thus favouring the diffusion of fuel cell vehicles. To achieve such objective, precious metal catalysts used in the electrolysis systems should be minimised and titanium bipolar plates possibly replaced by stainless steel treated with cheap coatings [8]. These strategies are currently addressed, but probably they may not be sufficient because it is still needed to take into consideration the cost of the balance of plant of the PEM electrolyser. This cost is strongly influenced by the hydrogen production rate [9].

On the other hand, it is widely recognised that the most relevant effect on decreasing the cost of PEM electrolysers will be played in the future by the increase of the operating current density while keeping the system efficiency at suitable levels [17–19]. When an electrolyser is operated in a high current density regime, the efficiency losses associated to the ohmic drop play a relevant role. In this regard, the proton transport in the polymer electrolyte membrane is producing a major contribution to the ohmic losses at high current density. Electronic percolation in the catalytic layers, diffusion media and bipolar plates contributes to ohmic losses in a lower extent [20,21].

Beside a high proton conductivity, proper mechanical strength and low gas-cross over under differential pressure operation are important characteristics that govern the reliability of the membrane separator between the anode and cathode compartments in PEM cells [8–13,22–25]. A decrease of the thickness of the polymer electrolyte membrane can allow to reduce the cell resistance but at the same time this increases the gas permeation from the pressurised hydrogen compartment to the non-pressurised oxygen stream at the anode [10–13]. An increase of the concentration of hydrogen in oxygen can cause relevant safety issues, the flammability limit being 4% vol. H_2 in O_2 at ambient temperature and pressure [26–32]. This requires adopting a compromise between the reduction of the membrane thickness to increase performance and the minimisation of the hydrogen concentration in the oxygen stream at practical operating current densities and differential pressures. Nafion® 117 with a membrane thickness of 170 μm and other thick proton exchange membranes usually guarantee for reasonably low gas crossover in the presence of differential pressures of a few tens of bars [10–13,27,28].

Short side-chain Aquivion® membranes have been first investigated in fuel cells because of their excellent ionic conductivity and low gas crossover thanks to the enhanced crystallinity and lower equivalent weight compared to conventional PFSA membranes [33–39]. These membranes also offer good capability to operate in a wider temperature range thank to their high glass transition temperature [34–37]. The use of Aquivion® membranes in PEM electrolysis [40–45] is gaining momentum in recent years while durability characteristics in electrolysis cells have been already assessed [18,19].

Beside the different mechanical and gas crossover properties, fabrication of the Aquivion® membranes, using extrusion or casting, has also an impact on cell performance. All these aspects are of paramount importance for the reliability of the PEM electrolysis system [40–45].

To discriminate between these effects, we have investigated Aquivion® membranes with equivalent weight of 980 g eq^{-1} and thickness of 90 μm, produced by extrusion or casting methods, with regard to their electrochemical performance and gas crossover characteristics in electrolysis cells. These membrane-electrode assemblies contained low precious metal loadings in accordance with the trend of decreasing the impact of critical raw materials on the overall cost of the PEM electrolysis system [19,46,47]. Interestingly, it was observed that the membrane fabrication method influences significantly the interfacial properties with the electrodes affecting the polarisation resistance and degradation rate in durability studies.

Electrolysis cells have been compared for operation at high current density (3–4 A cm^{-2}) as required to decrease significantly the capital costs of the electrolysis systems [18,19,48] while gas crossover was investigated during high differential pressure operation to examine the impact of the membrane fabrication method on the system safety.

2. Experimental

2.1. Membrane preparation

The commercially available extruded *s*hort-side chain Solvay Aquivion® membrane (E98-09S) with an equivalent weight (EW) of 980 g eq^{-1} and a thickness of 90 μm was prepared by melt extrusion of polymer resin in $–SO_2F$ form. Membrane thus obtained was treated with $NaOH/H_2O$ solution and then with HNO_3/H_2O transforming $–SO_2F$ in $–SO_3H$ group. A chemical stabilisation process was carried out on the raw polymer. The polymer resin was subjected to a post-fluorination of end groups with difluorine gas (F_2) at high temperature.

The recast *s*hort-side chain Solvay Aquivion® membrane (C98-09S) with an equivalent weight of 980 g eq^{-1} and a thickness of 90 μm was prepared starting from commercial water-based Aquivion® D98-25BS dispersion (EW: 980 g/mol, 25 wt% solid content). The Aquivion® dispersion was based on the same chemically stabilised polymer resin, as in the case of the extruded membrane, but already converted to the protonic form. This dispersion was formulated till obtaining the following composition: Aquivion® polymer (22 wt%), deionized water (36 wt%), *n*-propanol (32 wt%) and *N*-methylpyrrolidinone (10 wt%). The dispersion thus obtained was cast on tempered glass using a doctor blade (Zehntner ZUA2000) and an automatic applicator (Zehntner ZAA2300). The wet thickness used for casting the Aquivion membrane® was set at a gap of 900 μm. After deposition, the film underwent a three-steps heating cycle in a vent oven: 1 h at 65 °C, 1 h at 90 °C and 1 h at 190 °C. The ionomer was used in the protonic form during casting and annealing. Membrane was then peeled off from glass using demineralized water. It was dried in a vent oven at 80 °C.

The final thickness used for calculation of conductivity values, was measured according to a United States Department of Energy (DOE) protocol (DOE Contract # DE-FC36-06GO16028, Florida Solar Energy Center 1679 Clearlake Road Cocoa, FL 32922-5703; June 9, 2008). The membrane sample was placed on a clean counter surface and allowed to equilibrate for 24 h at a room temperature of 21 °C and average room relative humidity of 60%. A Mitutoyo Gauge was used to determine the sample thickness. An average of at least 10 readings were taken over the entire membrane sample.

2.2. In plane conductivity

The electrochemical measurements were performed at 80 °C with a four-point-probe Bekk-Tech BT-112 conductivity cell. Humidified hydrogen (1000 sccm supplied at the anode side of the cell) and heating were provided by a Greenlight Power Technologies FCATS-E 1 kW fuel cell test bench. The electrical connection was made to an Autolab PGSTAT-30 potentiostat/galvanostat (Metrohm). In-plane conductivity was measured in a relative humidity window from 20% to 120% R.H. Cell resistance was determined as slope of cell voltage vs. current; conductivity was calculated considering the resistance value and geometrical parameters of sample. System was conditioned at the operating temperature for 1 h prior data acquisition.

2.3. Water uptake and dimensional swelling

Die-cut (7 × 7 cm^2) samples were dried in a vacuum oven at 105 °C for 1 h. Thereafter these were carefully weighed and their dimensions (length, width and thickness) measured (M_{dry}). Membranes were then soaked in demineralized water at 80 °C for 4 h, cooled down at room

temperature and, after wiping water droplets from the surface, weighed and the dimensional changes measured (M_{wet}). Water uptake and dimensional swelling were calculated accordingly to equation (1):

$$Water\ Uptake\ \&\ Dimensional\ Swelling = \frac{M_{wet} - M_{dry}}{M_{dry}} * 100 \quad (1)$$

2.4. Stress-strain analysis

Stress-strain curves were recorded with an Instron 5500R dynamometer equipped with a Bluehill 2 software at 23 °C, 50% RH, traction speed from 1 to 50 mm/min and measuring specimens having dog bone shape (initial length: 21.5 mm and grip distance: 25.4 mm) according to ASTM D633 type V protocol. The water content of the membranes used in the tensile tests was 6 % wt. Reported curves represent mean values of measurements repeated at least 3 times.

2.5. Membrane-electrode assembly preparation and characterisation

An Aquivion® ionomer dispersion (D98-06AS, EW: 980 g/mol., 6 wt % solid content in hydroalcoholic medium, chemically stabilised) was used to prepare the catalytic inks. Extruded and recast short-side chain Solvay Aquivion® membranes were spray-coated by catalytic inks based on an IrRuOx (70:30 at.) anode catalyst on one side and a 30% Pt/C (Ketjenblack® carbon) cathode catalyst on the opposite side of the membrane. The membrane side that was cast on the glass substrate was coated with the cathodic ink during the catalyst-coated membrane preparation.

Catalysts characteristics have been reported in a previous paper [20]. Catalyst-coated membranes (CCMs) were hot-pressed at 190 °C for 1.5 min at 11.2 kN to achieve proper bonding of the catalytic layers to the membrane. The inks made of catalyst and ionomer consisted of 75 % wt. Pt/C catalyst and 25% wt. Aquivion® ionomer at the cathode, and 85 % wt. IrRuOx catalyst and 15% wt. Aquivion® ionomer at the anode. The precious catalyst loadings were 0.4 mg IrRuOx cm^{-2} and 0.1 mg Pt cm^{-2} at anode and cathode, respectively.

For electrochemical testing at ambient pressure, the CCM was in contact with a Ti mesh (Bekaert Toko Metal Fiber Co.) at the anode and a carbon cloth-based diffusion layer at the cathode. Whereas for high-pressure measurements (20 bar), Ti meshes were at both sides of the CCM for current collection and water distribution/gas diffusion. An in-house designed square-shaped titanium plates-based single cell test fixture of 5 cm^2 active area, equipped with machined flow fields, was used for electrochemical experiments at ambient pressure. High-pressure measurements were carried out with a circular-shaped pressurised single cell test fixture of 8 cm^2 active area supplied by ITM Power (Sheffield, UK). Two different test stations designed for ambient pressure and high-pressure electrolysis operation, respectively, were used to assess the MEA properties.

Polarisation experiments were carried out by using computer controlled power supply modules (TDK GEN 25-400-MD-3P400). Electrochemical impedance spectroscopy (EIS) was performed with an Autolab Metrohm potentiostat/galvanostat equipped with a 20 A current booster and FRA (frequency response analyser). Polarisation curves were recorded in the galvanostatic mode by registering the cell voltage vs. the imposed current density. Electrochemical impedance analysis was carried out in the potentiostatic mode at 1.5 V and 1.8 V. The frequency was varied from 100 kHz to 100 mHz in the single sine mode with a sinusoidal excitation signal of 10 mV rms. Deionized water, milli-Q Integral, Millipore was fed to the anode compartment only.

The MEA cross-section was analysed by a scanning electron microscopy (SEM) using a FEI FEG–XL30 instrument. For AFM investigations, small pieces of membrane samples were cut from 90 μm thick PFSA Aquivion® E98-09S and C98-09S films. The samples were fixed to the sample holder by an adhesive tape. A Multimode Veeco microscope controlled by a Nanoscope IIIa software was used. For image acquisition, the tapping mode method was used by registering height, amplitude and phase. A Bruker RTESP tip was employed (r = 8 mm, f = 300 kHz; k = 40 N/m). Images were acquired with a resolution of 512 × 512 pixels and elaborated using the Gwyddion 2.31 software. Surface roughness (R_a) was determined as follows (equation (2)):

$$R_a = 1/L \int_0^L |Z(x)| dx \quad (2)$$

Where Z(x) is the profile function that describes the height and position on the line scan L. This calculation was carried out for all image lines.

2.6. Oxygen permeation studies

For the oxygen permeation studies, membrane-electrode assemblies (MEAs) were produced using the E98-09S and C98-09S membranes under study and fabricated according to the same method reported for the electrolysis MEAs. As in the case of the electrolysis MEAs, Pt/C cathode catalyst layer and IrRuOx anode catalyst layer were used with the same percentage of ionomer in the catalytic layer. The only variation was a higher Pt cathode loading of 0.45 mg cm^{-2}. A 25 cm^2 active area single cell was used. The oxygen permeability (PO_2) was assessed from the limiting current density (oxygen crossover rate limited) of the oxygen reduction reaction (ORR) at the cathode, as expressed by the following formula (equation (3)):

$$P_{O2} = \frac{i_{ORR} \cdot \delta_{mem}}{4F \cdot pO_2} \quad (3)$$

where i_{ORR} is the oxygen reduction reaction current, δ_{mem} is the membrane thickness, F is the Faraday constant (96487C mol^{-1}) and pO_2 is the oxygen pressure.

The measurement procedure consisted in a first step of conditioning for 4 h in H_2/air at a cell temperature of 75 °C and a relative humidity of 65%; after that, the system was purged in N_2 at the same temperature. The measurement was then carried out at a 60 °C, feeding humidified N_2 (cathode) and humidified O_2 (anode) at pressure of 120 kPa, O_2 flow rate of 1000 sccm, N_2 flow rate of 500 sccm, 100% R.H. and a fixed potential of 1 V was applied using an AutoLab PGSTAT30 potentiostat/galvanostat equipped with the program Nova 2.1.

3. Results and discussion

3.1. Ex-situ membrane characterisation

3.1.1. In-plane conductivity

In-plane conductivity has been measured at 80 °C and in the relative humidity range from 20% to 120% R.H. (Fig. 1).

Both membranes, having the same equivalent weight (980 g/mol.), show a similar trend. As expected, proton conductivity increases by increasing relative humidity. Both membranes reach the same value of 130–140 mS cm^{-1} under full humidification. This result clearly show that the manufacturing process does not affect the ion conduction properties of Aquivion® membranes under full humidification which are determined by the amount of $-SO_3H$ functional groups and their dissociation. At low R.H. values (20%) the extruded membrane shows larger conductivity. However, this condition is less relevant for electrolysis applications.

The effect of the machine direction during melt extrusion is usually important when hydrolysis is done in a roll-to-roll process. Stretching of the wet, softened membrane and drying between the rolls, leading to constraining forces, may also have some influence on the final membrane properties. In the case of the extruded membrane, the ionic conductivity measurements have been carried out in both machine (MD) and transversal (TD) directions. However, the observed variations were within the experimental error. Possibly, the distribution of the ion

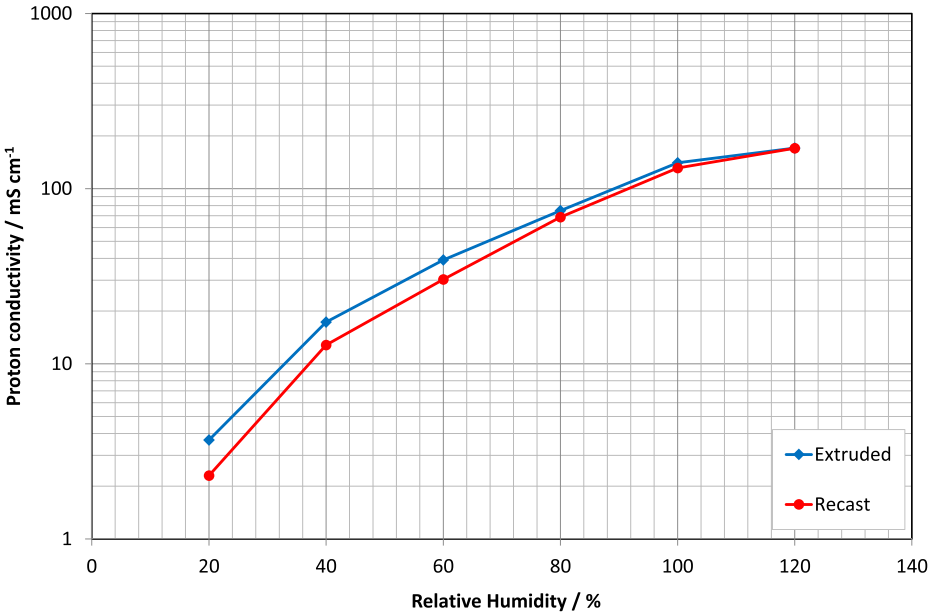

Fig. 1. In-plane proton conductivity at 80 °C vs. relative humidity of extruded (E98-09S) and recast (C98-09S) membranes.

clusters inside the membrane is not significantly different along these directions.

3.1.2. Water uptake and dimensional swelling

Membrane water uptake and related dimensional changes have been determined upon sample soaking in hot deionized water (Fig. 2). The dry thickness of the membrane was 90 ± 5 µm.

Although having the same EW, extruded membranes show a higher water uptake than recast ones, 33% *vs.* 26%, corresponding to 19 and 15 water molecules per sulfonic acid group, respectively. In addition, dimensional swelling is strongly influenced by the manufacturing process. Extruded membranes show different volume change in the three dimensions whereas recast membranes swell more homogeneously upon hydration. This different behaviour is ascribed to the higher anisotropy induced to membranes from melt extrusion than dispersion casting process [49]. In particular, change in length is predominant because of the membrane stretching in machine direction during melt extrusion.

The higher conductivity of the extruded membrane versus the recast membrane observed at low R.H. in Fig. 1 may be thus related to the different water uptake behaviour and related swelling properties of these polymer electrolytes. The extruded membrane which is characterised by larger water uptake and higher increase in swelling properties, in terms of length and width, shows better conductivity at low R.H.

Fig. 2. Water uptake and dimensional swelling of extruded (E98-09S) and recast (C98-09S) membranes upon soaking in deionized water (80 °C, 4 h).

3.1.3. Stress-strain mechanical measurements

Stress-strain curves of both recast and extruded membranes are reported in Fig. 3. Considering the higher anisotropy of extruded than recast membranes, mechanical tests of the former have been carried out in both machine (MD) and transversal (TD) directions.

Different properties are evident at macroscopic scale very likely as a result of a different nanoscale morphology for these two membranes (see below). The recast membrane shows the typical behaviour of a soft and weak polymer having lower elastic modulus and similar elongation at break of extruded membrane, which behaves as a hard and tough material. Anisotropy of extruded membrane is clear by comparing the stress-strain behaviour in machine and transversal direction (Table 1).

According to conductivity and mechanical measurements both membranes appear appropriate for electrolysis operation at high current density and high differential pressure. Recently, Cavaliere et al. [45] have shown that addition of a 5% electrospun polysulfone fibres in a recast reinforced Aquivion® membrane with 830 g eq^{-1} EW produces an enhancement of proton conductivity and mechanical strength. In our case, we have selected the Aquivion ionomer with 980 g eq^{-1} EW to reduce hydrogen cross-over at high differential pressure operation of 20 bar (see below) as pre-requisite to reduce membrane degradation during long term electrolysis operation.

3.2. Electrochemical characterisation

Polarisation curves of PEM electrolysis MEAs based on extruded and recast Aquivion® membranes have been carried in a wide range of temperature (from 30 to 90 °C) and current density (up to 4 A cm^{-2}) with a reduced overall precious catalyst loading (0.5 mg cm^{-2}_{MEA}). Operation at high current density and using low loading of precious metals, can allow for a significant reduction of the capital costs of the PEM electrolysis system [18,19]. In this regard, it is important to understand which membrane characteristics are most appropriate for operation under such conditions.

In principle, an electrolysis stack, being operated in a pressurised mode in the real life, could operate also at temperatures above 100 °C. This was already demonstrated for PFSA membrane-based electrolysis

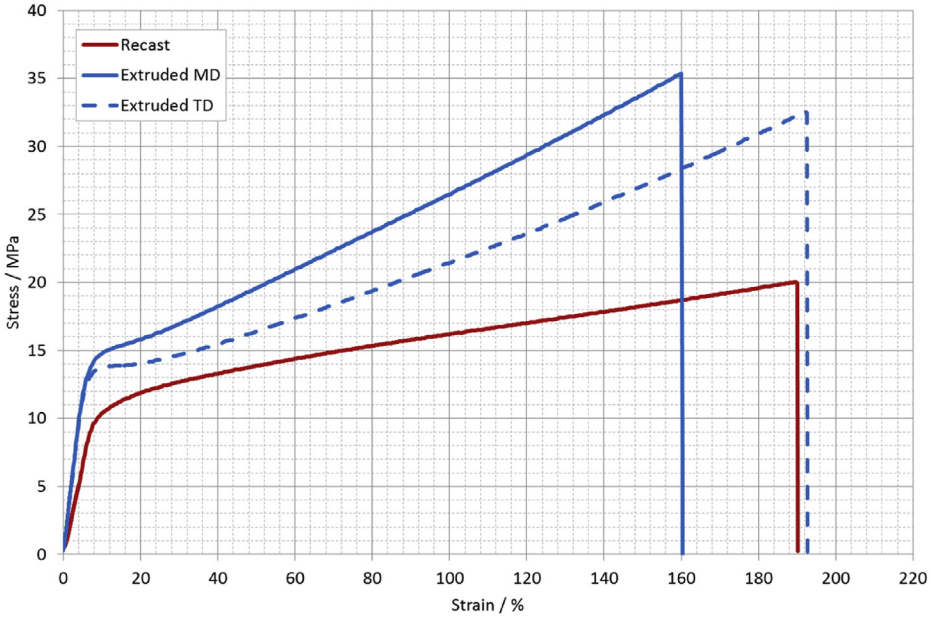

Fig. 3. Stress-strain curves of recast (solid red), extruded MD (solid blue) and extruded TD (dashed blue) membranes. MD: Machine Direction; TD: Transversal Direction. (For interpretation of the references to colour in this figure legend, the reader is referred to the Web version of this article.)

Table 1
Characteristic features of extruded and recast Aquivion® membrane. MD: Machine direction; TD: Transversal Direction.

	Modulus (MPa)	Stress at Break (MPa)	Strain at Break (%)
Recast	189 ± 23	21.6 ± 1.4	184 ± 14
Extruded (MD)	301 ± 39	36.3 ± 1.6	162 ± 3
Extruded (TD)	273 ± 10	32.5 ± 2.0	187 ± 17

cells [42,50]. However, conventional PEM electrolysis systems usually operate at low temperatures e.g. 55–60 °C to mitigate stack degradation thus assuring proper system life-time. Other limitations are essentially regarding the balance-of-plant [9]. These have also limited the possibility of high temperature operation for commercial systems. However, it is widely accepted that an increase of operating temperatures can bring significant benefits in performance and efficiency [42,50].

The polarisation curves for the electrolysis cell based on the extruded membrane (Fig. 4a) show a relevant increase of current density (hydrogen production rate) with temperature at a fixed cell voltage (voltage efficiency). This clearly evidences the benefits of operating the electrolyser at high temperature in increasing the cell efficiency. At 90 °C, a current density of 4 A cm^{-2} is obtained at 1.85 V with an overall noble metal catalyst loading (Ir + Ru + Pt) of 0.4 mg cm^{-2} and a membrane thickness of 90 μm.

In a practical electrolysis system, the stack is self-heating during normal operation. During cold start, at suitable current density, the cells operate above the thermoneutral potential where the reaction is exothermic. In principle, water splitting cannot occur below the thermoneutral potential corresponding to the reaction enthalpy ($\Delta H^\circ/nF = E_{tn}$) if no external heat is provided. In our experiments, we have thermostated the cell inlet water at specific temperatures, thus providing an external heat input. This approach provides part of the heat theoretically required by the reaction entropy (reversible heat, $Qrev = T\Delta S^\circ$) thus shifting the onset potential for the water splitting process towards the reversible potential ($E_{rev} = \Delta G^\circ/nF$). During operation at high current density and well above the thermoneutral potential, all the reversible heat is provided by the internal production of thermal energy as consequence of the exothermic process. Extraction of the heat is easier at high temperature; whereas, at low temperature a cumbersome cooling system is necessary. Thus, a relatively high operating temperature, compatible with the balance of plant and stability constraints, is of relevant interest for the electrolysis cell [42,50].

The polarisation curves show a reduction of the activation losses (cell voltage increase in the low current density region) and ohmic constraints (slope of the polarisation curves at high current densities) with the increase of temperature (Fig. 4a). This clearly evidences that high hydrogen production rates in combination with suitable voltage efficiencies (e.g. 4 A cm^{-2} at about 85% voltage efficiency vs. the thermoneutral potential) can be essentially achieved when the system is operated at relatively high temperatures (80–90 °C).

Electrochemical impedance analysis was carried out under a constant voltage efficiency condition (Fig. 4b–c). This provides insights into the effects related to the variation of the reaction rate with the temperature. The possibility of achieving high reaction rates at fixed cell voltages is inversely related to series resistance (high frequency intercept on the real axis of the Nyquist plot) and polarisation resistance (difference between the lowest frequency impedance and the high frequency intercept resistance). These parameters allow to simply distinguish between ohmic losses and specific electrode polarisations. In all impedance experiments here recorded, the inductance effects usually produced by the cables were not significant. Thus, the series resistance, i.e. the impedance intercept on the real axis of the Nyquist plot (zero phase shift) at high frequency, also represents the high frequency resistance (HFR).

The ac-impedance spectra in the low voltage region (1.5 V) show that the overall cell impedance shifts from 1.75 Ohm cm^2 to 0.125 Ohm cm^2 as the temperature is increased from 30 °C to 90 °C (Fig. 4b). At low temperatures, most of the impedance contribution is from the polarisation resistance (electrodes contribution); whereas, at 90 °C, the series resistance contribution, associated to the ohmic losses (Fig. 4b and inset), is prevailing with respect to the polarisation resistance.

At 1.8 V, the prevailing contribution of the series resistance is clearly observed at all temperatures. Under such conditions, the contribution of the polarisation resistance to the overall impedance is about 20% at 60 °C and about 10% at 90 °C. This reveals that at high currents the differential resistance in the polarisation curves is essentially corresponding to the membrane resistance (assuming electronic percolation in the catalyst layers and the current collectors as optimal). Thus, the membrane plays the major role in determining the performance at high current density.

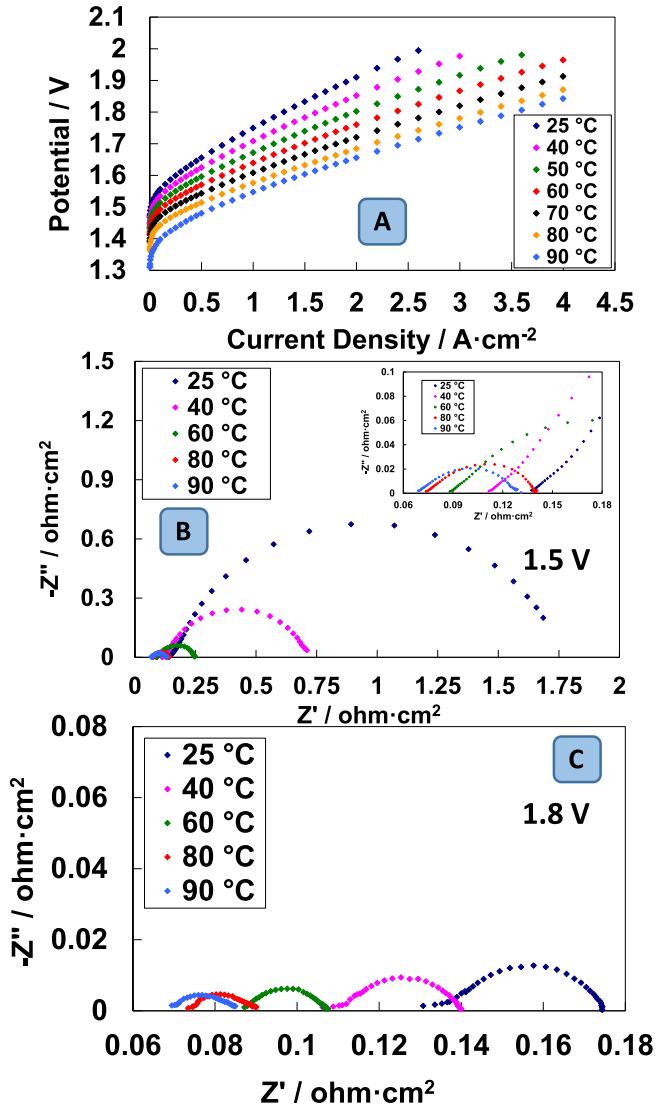

Fig. 4. Polarisation curves (a) and ac-impedance spectra at 1.5 V (b) and 1.8 V (c) at different temperatures for the MEA with extruded membrane.

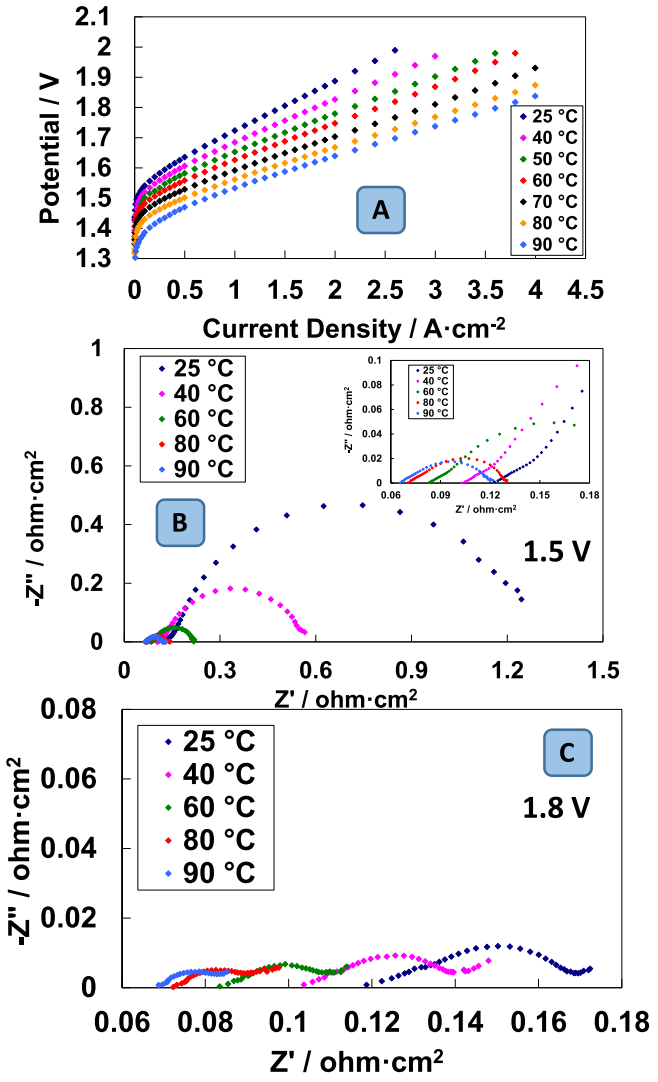

Fig. 5. Polarisation curves (a) and ac-impedance spectra at 1.5 V (b) and 1.8 V (c) at different temperatures for the MEA with casted membrane.

The recast membrane shows polarisation characteristics similar to the extruded membrane-based MEA (Fig. 5a). However, the EIS spectra at 1.5 V (Fig. 5b) shows, at low temperature, a relevant difference, i.e., the overall impedance is about 1.3 Ohm cm^2 for the recast membrane versus 1.75 Ohm cm^2 for the extruded polymer-based MEA under the same conditions. This essentially derives from a larger polarisation resistance in the case of the extruded membrane (1.61 *vs.* 1.18 Ohm cm^2). Similar evidences are observed in the impedance spectra collected at low temperature at 1.8 V (Fig. 5c). Having used the same electrodes, catalyst and ionomer loadings in both MEAs, this difference is ascribed to the different interfacial properties arising from the different membrane characteristics.

It is observed that both MEAs offer excellent performance at high current densities and high temperature with a voltage efficiency versus the thermoneutral potential of about 85% and 80% at 3 and 4 A cm^{-2} at 90 °C.

A comparison of the polarisation curves at 80 °C for the two MEAs (Fig. 6a) shows a small but evident activation enhancement in the case of the recast membrane resulting from a lower polarisation resistance at 1.5 V (Fig. 6b). A very good reproducibility was observed for these initial polarisation curves by investigating different sets of the same MEAs. This indicates that the observed differences are specifically related to the membrane used in the MEA.

The series resistance is just slightly lower for the recast membrane according to the fact that both membranes are based on the ionomer and have the same thickness. At 1.8 V (Fig. 6c), it seems that some small additional low frequency contribution is present in the case of the recast membrane as envisaged from the presence of the onset of a low frequency semicircle or possibly a Warburg-like diffusion-related contribution. As consequence of the different differential resistances, the extruded membrane recovers the performance gap with the recast membrane at 4 A cm^{-2} showing the same voltage efficiency.

An analysis of the variation of the various impedance contributions to total resistance (R_{tot}) as function of temperature for the two MEAs (Fig. 7 a-d, Table 2 and Table 3) shows clearly that, at low cell voltages or low current densities (Fig. 7a–b and Table 2), the polarisation resistance (R_p) is dominating below 60 °C. Whereas, at high cell voltages or high current densities (Fig. 7 c-d and Table 3), the series resistance is largely prevailing at all temperatures. The series resistance (R_s) is slightly lower in the case of the recast MEA under all conditions (Fig. 8). The polarisation resistance is lower at low voltages for the recast membrane-based MEA but the trend is inverted at 1.8 V. At 80–90 °C, both polarisation and series resistance appear very similar for the two membranes (Figs. 7 and 8) in accordance with the performance overlapping of the polarisation curves (Fig. 6).

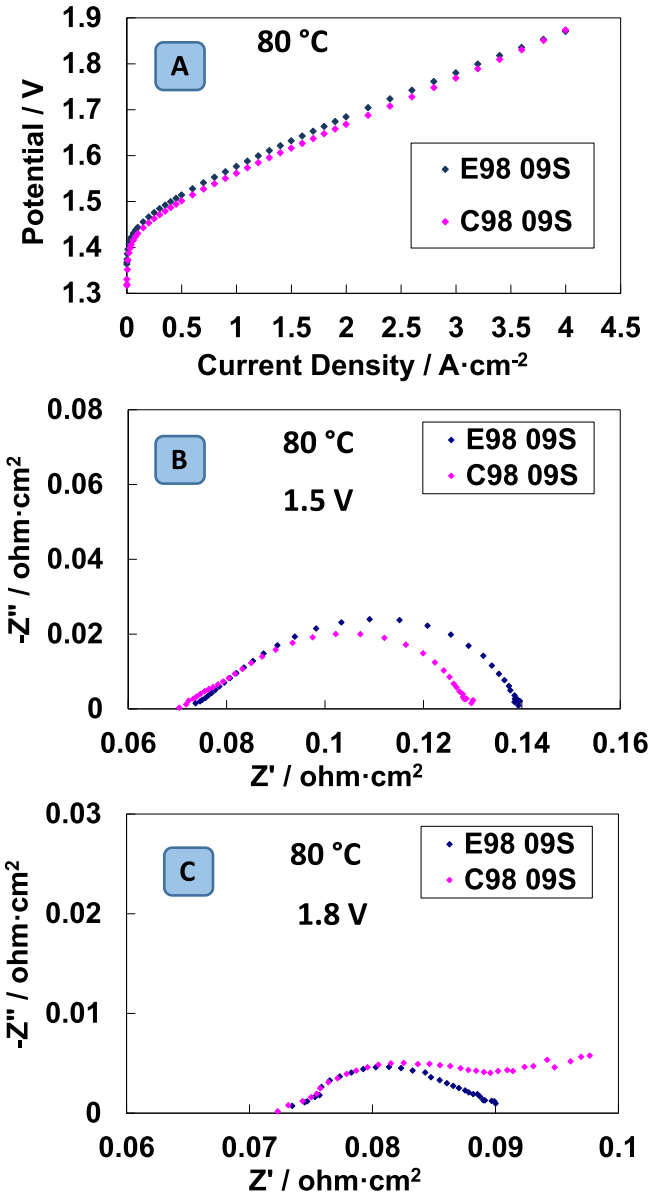

Fig. 6. Polarisation curves (a) and ac-impedance spectra at 1.5 V (b) and 1.8 V (c) at 80 °C of the MEAs with extruded and casted membranes.

3.3. Durability tests

The MEAs based on the extruded and recast membrane were subjected to a durability test (Fig. 9). This was consisting in a cell conditioning at 1 A cm^{-2} before a switch to a current density of 3 A cm^{-2}. At 1 A cm^{-2} both cells gave rise to a rapid cell voltage increase in the first hours of operation (reversible losses associated to mass transport constraints) followed by a gradual increase of voltage with time (Fig. 9). As previously noted from the polarisation curves and EIS spectra, the performance of the recast membrane-based MEA was slightly better at low current density (lower cell voltage corresponding to higher voltage efficiency) than that of the extruded membrane-based MEA. This is reflected in a slightly lower cell voltage at 1 A cm^{-2} in the durability studies (Fig. 9). After the switch from 1 to 3 A cm^{-2}, both cells showed the same initial cell voltage. However, the MEA based on the extruded membrane showed a clear increase of potential with time. On the contrary, the cell voltage for the recast membrane-based MEA remained almost constant with time (Fig. 9).

The extruded membrane-based cell was subjected to a few shutdown and start-up cycles, during the operation period between 500 and 1000 h (Fig. 9). This was made to check for the occurrence of reversible losses. It seems that the system is able recovering in part its initial performance. This suggests that a relevant part of this voltage increase is essentially due to some reversible losses arising probably from mass transfer issues related to the gas evolution [51,52]. A similar approach was used for the recast membrane-based MEA. It was observed that the reversible losses are also present in the durability curve of the recast membrane-based MEAs. However, their impact on the variation of the cell potential appears smaller than that observed for the extruded membrane. Since the recast membrane-based MEAs showed excellent stability at 3 A cm^{-2}, after about 1300 h operation, its durability was investigated also at 4 A cm^{-2}. The stability was good also under these conditions. However, after a few shutdown and start-up cycles in the period between 1300 and 2000 h, this system showed slightly larger recoverable losses, i.e. increase of cell potential, than at 3 A cm^{-2}. These recoverable losses were, in any case, much smaller than those observed for the extruded membrane.

According to our previous studies [19], the degradation rate is exacerbated by both the low catalyst loading and the high operating current density. The performance decay that has been registered in the experiment here carried out at 3 A cm^{-2} for the extruded membrane after 1000 h operation, i.e. in the region where no shut-down/start-up cycles were made, was about 30 μV/h. This appears slightly larger than what we have observed in previous durability studies with relatively similar MEAs in the presence of low catalyst loadings (24–26 μV/h) [18–20]. However, the most relevant aspect is that there is a significantly different durability profile for the MEAs consisting of recast and extruded membranes (6 vs 30 μV/h at 3 A cm^{-2} in the regions of the durability curves not subjected to shut-down cycles). In principle, this should be originated from the different interfacial properties with the catalytic layers for the two membranes.

In addition, it should be also considered that the swelling is different for the two membranes. As observed above extruded membranes swell more than recast membranes both in length and width (Fig. 2). This could lead to a higher number of slightly delaminated areas for the extruded membrane, which then would fill with gas causing additional mass transfer issues.

3.4. Morphological studies

To better understand the role of the membrane on the interfacial characteristics, morphological studies were carried out by both scanning electron microscopy (SEM) of the MEAs cross-sections and atomic force microscopy of the membrane surface.

The MEAs were simply cut in the middle with a knife without any further polishing procedure. A good adhesion of the electrodes to the membrane was observed in the SEM analysis of the fresh MEAs cross-sections (Fig. 10a–b). Both anode and cathode layers appear compact but also characterised by a good porosity. This porosity is also deriving by the formation of an intimate mixture between the catalyst powder and the Aquivion® ionomer dispersion. The ionomer inside the catalytic layers, having the same composition of the membrane, plays a paramount role in favouring an electrode bonding to the membrane. This is also enhanced by the hot pressing treatment of the MEA at a temperature higher than the Aquivion® glass transition temperature. Despite the precious metal loading is much lower at the cathode, the thickness of this catalytic layer is not significantly lower than that of the anode because Pt is supported on a high surface area carbon characterised by high specific volume whereas the anode catalyst is unsupported. The SEM cross-section of the recast MEA, after almost 2500 h operation, shows some delamination at the cathode (Fig. 10c). However, this is simply because the cathode layer sticks more strongly to the diffusion layer backing than the membrane and, during the cell dismantling, this gives rise to a delamination from the membrane. Also part of the anode particles remained in the Ti foam after cell

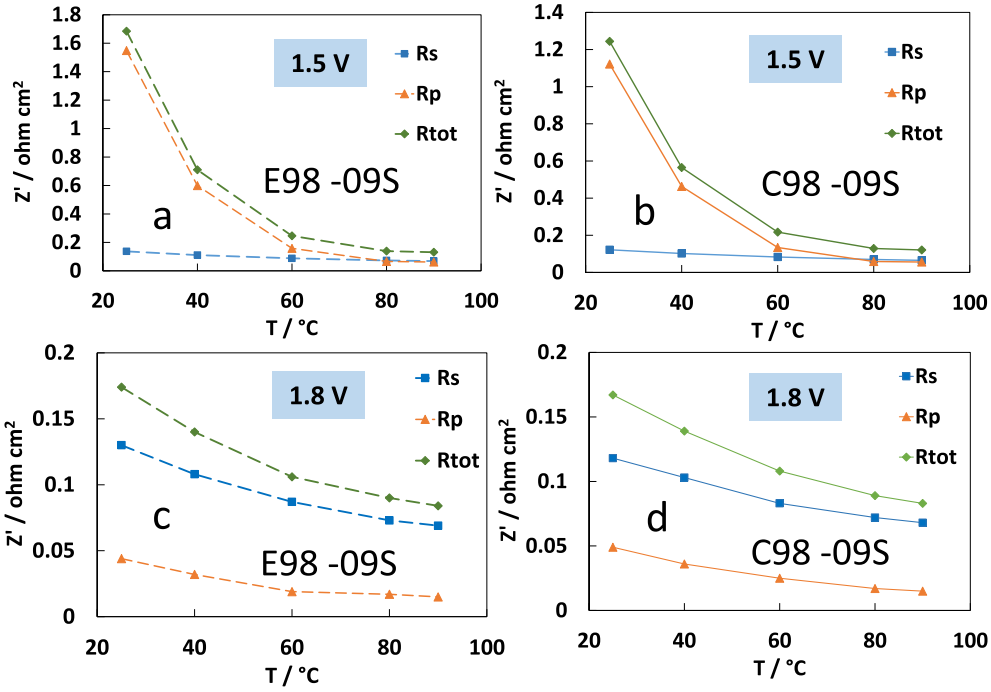

Fig. 7. Impedance contributions as function of temperature at low (a,b) and high voltages (c,d) for the extruded (a,c) and recast (b,d) membrane-based MEAs as function of temperature.

Table 2
Impedance parameters as function of temperature at 1.5 V for the extruded E98-09S and recast R98-09S membrane-based MEAs as function of temperature.

Cell Potential 1.5 V	Extruded E98-09S membrane			Casted C98-09S membrane		
T/°C	$R_s/\Omega\ cm^2$	$R_p/\Omega\ cm^2$	$R_{tot}/\Omega\ cm^2$	$R_s/\Omega\ cm^2$	$R_p/\Omega\ cm^2$	$R_{tot}/\Omega\ cm^2$
25	0.137	1.548	1.685	0.122	1.122	1.244
40	0.111	0.599	0.710	0.102	0.463	0.565
60	0.088	0.158	0.246	0.083	0.134	0.217
80	0.073	0.066	0.139	0.070	0.059	0.129
90	0.069	0.062	0.131	0.065	0.056	0.121

Table 3
Impedance parameters as function of temperature at 1.8 V for the extruded E98-09S and recast R98-09S membrane-based MEAs as function of temperature.

Cell Potential 1.8 V	Extruded E98-09S membrane			Casted C98-09S membrane		
T/°C	$R_s/\Omega\ cm^2$	$R_p/\Omega\ cm^2$	$R_{tot}/\Omega\ cm^2$	$R_s/\Omega\ cm^2$	$R_p/\Omega\ cm^2$	$R_{tot}/\Omega\ cm^2$
25	0.130	0.044	0.174	0.118	0.049	0.167
40	0.108	0.032	0.140	0.103	0.036	0.139
60	0.087	0.019	0.106	0.083	0.025	0.108
80	0.073	0.017	0.090	0.072	0.017	0.089
90	0.069	0.015	0.084	0.068	0.015	0.083

dismantling.

The SEM images indicate for the fresh MEAs an intimate contact between the catalytic layer and the membrane ionomeric clusters. Thus, there are no relevant features that may allow to interpret the differences observed between these MEAs in the durability studies.

An AFM analysis in the tapping mode was thus carried out on the outer surface of the membranes only. The aim was to get insights into the different surface roughness. Figs. 11 and 12 show the topographical images of the surface of Aquivion® membranes prepared by extrusion or casting procedures and designed for electrolysis applications. The extruded membranes showed similar morphology features on both faces whereas the casted membranes revealed just slight differences for the two faces as evident from the roughness analysis reported in Table 4. Essentially, one face of the recast membrane is slightly affected by the characteristics of the substrate where the membrane was deposited. This is especially evident at a macroscopic scale. As reported in the experimental part, the membrane side casted on the glass substrate was coated with the cathodic ink during the catalyst-coated membrane preparation.

The AFM images on the smaller scale (1 μm × 1 μm) show the supermolecular structure of the membrane (Figs. 11 and 12). Typically, this is made of spherical grains of a diameter in the range of tens nanometers surrounded by interstitial regions of smaller thickness. On the larger scales (10 μm × 10 μm and 50 μm × 50 μm), the macroscopic properties of the membrane surface are visualised (Figs. 11 and 12).

Several AFM studies of the PFSA membranes have been reported in the literature [53–56]. This technique has allowed visualising the membrane morphology at high magnification without causing significant degradation contrary to what occurs with electron beams. The polymer chains of the PFSA systems consist of a perfluorinated backbone with side chains bringing terminal ionic groups. This structure gives rise to a phase separation during membrane fabrication. The sulfonated ionic clusters of the hydrophilic ionic phase allow proton conduction in the presence of water through this interconnected network. These features can be recognised using the AFM technique. The polymer chains of Aquivion® have been reported to be more crystalline than Nafion® [33]; these form dense bundles of some nanometers size providing mechanical strength to the polymeric film [53–56].

The properties of the Aquivion® membrane with equivalent weight of 870 EW have been widely investigated for fuel cell applications by Hiesgen et al. [55,56]. The lamellar structure of the fluorocarbon chains in Aquivion® and the ionic side groups distribution was studied in great detail [55,56]. Under equilibrium conditions, a surface morphology made of a lamellar stacking of backbone sheets and ionic side groups was observed. Not many AFM studies have been yet reported on Aquivion® membranes with equivalent weight of 980 eq g^{-1} and 90 μm

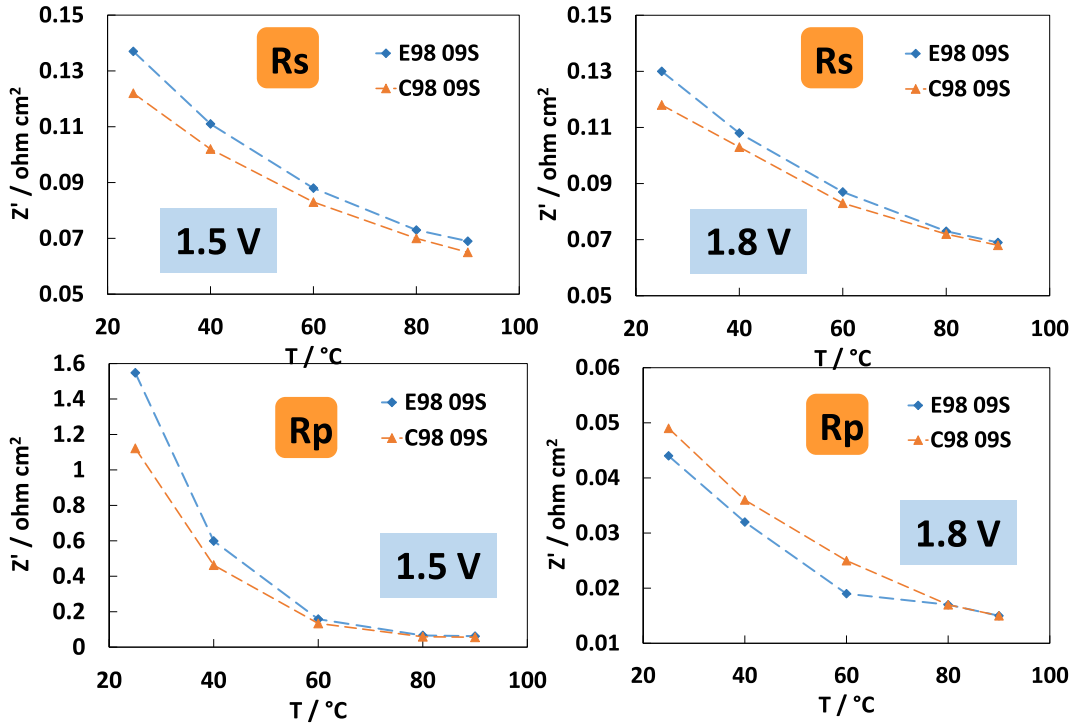

Fig. 8. Comparison of the series (Rs) and polarisation (Rp) resistance for the extruded and recast membrane based MEAs as function of temperature.

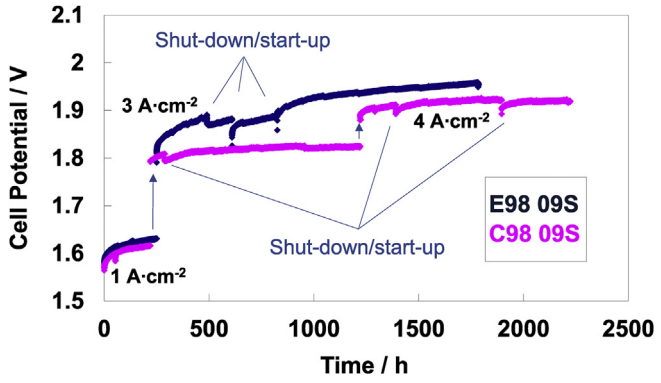

Fig. 9. Durability tests at 1, 3 and 4 A cm^{-2} and 80 °C for two different membrane-based MEAs in the water electrolysis cell.

thickness specifically designed for electrolysis application. These features are shown in Figs. 11 and 12.

In general, the topographical images of both membranes show the typical surface characteristics already evidenced by Hiesgen et al. [55,56] for Aquivion® polymers of lower EW used in fuel cell applications. However, a significant difference in surface roughness was observed between the extruded membranes and recast membranes. The AFM images showed a significantly higher surface roughness (R_a) for the extruded than the casted membrane, at both sides (Table 4). The roughness of the extruded membrane was more than three times that of the casted membrane at both 1 μm and 10 μm scales; it was also larger at the 50 μm scale. It is observed that the membrane water uptake and its related dimensional swelling, in terms of length and width, are also larger for the extruded membrane. It is hypothesised that these properties may be correlated and they influence the different conductivity behaviour at low R.H. (Fig. 1).

The presence of larger pores and voids in the extruded membranes surface would suggest that more catalyst could penetrate inside the membrane outer layers during the hot pressing MEA fabrication step. This in principle would suggest a larger extension of the catalyst-electrolyte interface [57] but, indeed, it may result in a lower intimate contact between the nanometre-sized catalyst agglomerates and the ionomer clusters of the membrane [55]. Moreover, since the membrane is a much more dense material than the catalyst-ionomer composite layer (see SEM images of the cross-sections in Fig. 10), the gas generated at the interpenetrated interface can escape less easily causing mass transfer issues that reflect into the larger reversible losses [51]. These are observed in a larger extent in the durability study of the extruded membrane-based MEA. It appears that the different surface properties of the membranes affect in some extent the activation characteristics of the MEAs in the polarisation curves (pseudo-steady state behaviour) producing better performance in the low current density region for the recast membrane-based MEA. The surface roughness appears to influence in a greater extent the evolution of the cell voltage with time, at high current density, during the steady-state durability tests showing lower reversible losses, or lower cell voltage rise with time, in the case of the recast membrane-based MEA.

Another important effect is related to the difference in swelling for the two membranes. As mentioned above the larger swelling occurring in the extruded membrane could lead to a higher number of slightly delaminated areas that upon filling in with the produced gas can give rise to mass transfer issues.

3.5. Hydrogen crossover under differential pressure

The MEAs based on the extruded and recast membranes were also characterised in terms of hydrogen permeation during electrolysis operation at high differential pressure. For specific power-to-gas applications where hydrogen is injected into the natural gas grid, a moderate operating pressure is sufficient for the electrolysis system [9]. Generally, the natural gas grid operates at a pressure lower than 10 bar at a local level. However, for electrolysis applications in refuelling stations, a large pressure is appropriate to reduce the energy consumed in the downstream mechanical compression of the hydrogen gas [8,9].

A large operating pressure for the PEM electrolysis system is characterised by some drawbacks especially in terms of a more expensive stack and balance of plant. The increased stack cost derives from the

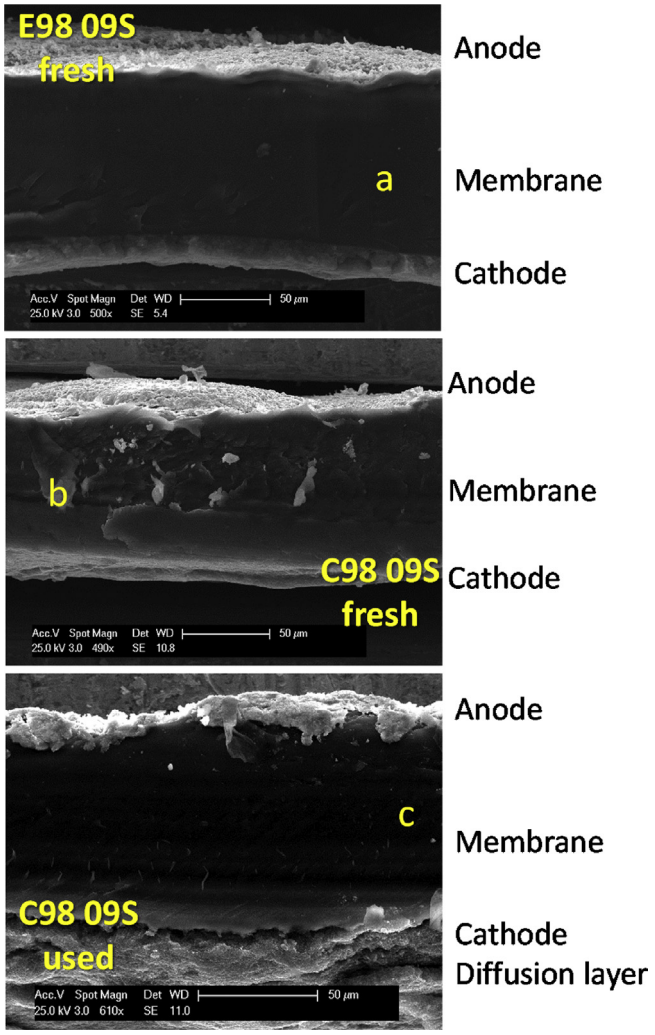

Fig. 10. SEM cross-sections of the fresh extruded (a) E98-09S and casted (b) membrane as well as of the used casted membrane after about 2500 h operation at high current density (3–4 A cm^{-2}) (c).

more demanding materials properties (special coatings to avoid H_2 embrittlement), stack design and sealing [12]. Other drawbacks concern with the increased energy consumption by the auxiliary equipment and the loss of faradaic efficiency. Usually, most of the conventional electrolysers operate between 20 and 30 bar [9]. Thus, the MEAs based on the extruded and recast membranes were operated at 20 bar differential pressure (pressurised hydrogen and non-pressurised oxygen). The concentration of hydrogen in the oxygen stream at the anode, permeation rate and faradaic efficiency were compared for the two membranes as a function of the operating current density. The estimation of hydrogen cross-over rate under high differential pressure operation provides useful information about the practical applications of these polymer membranes in electrolysis systems [58–61].

The concentration of permeated hydrogen in the oxygen stream at the anode (Fig. 13), is comparable for the investigated MEAs, in a wide range of current densities (1–4 A cm^{-2}). Although the flammability limit is 4% vol. H_2 in O_2 at ambient pressure and temperature [10,11,27,31], it is not appropriate exceeding a concentration of 3% vol. H_2. More specifically, the lower explosion limit of H_2 in oxygen has been estimated in 4.0% at 20 °C and 1.0 bar, 3.8% at 80 °C and 1.0 bar, and 5.2% at 80 °C and 20.0 bar [62,63]. Inset of Fig. 13 shows the increase of H_2 fraction in O_2 in a temperature window from 60 to 80 °C at 4 A cm^{-2}; hydrogen concentration increases of 0.005 vol %/°C and is however well below the safety limit of 3 vol %. Considering a nominal current density of 3 A cm^{-2}, the minimum partial load operation for both extruded and recast membranes is about 20%, i.e. 600 mA cm^{-2}. This is the minimum operating current density at 20 bars differential pressure. Such minimum partial load of 20% is similar to what is generally reported for conventional electrolysis systems (> 20%) [9,61]. Of course, if a nominal current density of 4 A cm^{-2} is selected, the minimum partial load operation can be as low as 15%. This may provide a slightly better flexibility for grid-balancing service [61]. The extruded membrane shows slightly lower gas permeation than the recast membrane at very low current density (0.15 A cm^{-2}) extending little bit the safety range compared to the recast membrane. As above discussed, the effect of melt extrusion can be relevant since stretching of the wet, softened membrane and drying between the rolls can give rise to constraining forces inducing membrane properties different than in the case of the recast membrane [64]. In both cases, the hydrogen crossover rate (Fig. 14a) does not affect significantly the faradaic efficiency (Fig. 14b) that remains above 99% in a wide range of operation, especially at high current densities, for both systems.

It is observed in Fig. 14a that the permeation of hydrogen increases progressively with the current density. This is very likely due to the increased supersaturation of H_2 in the cathode layer as a function of the

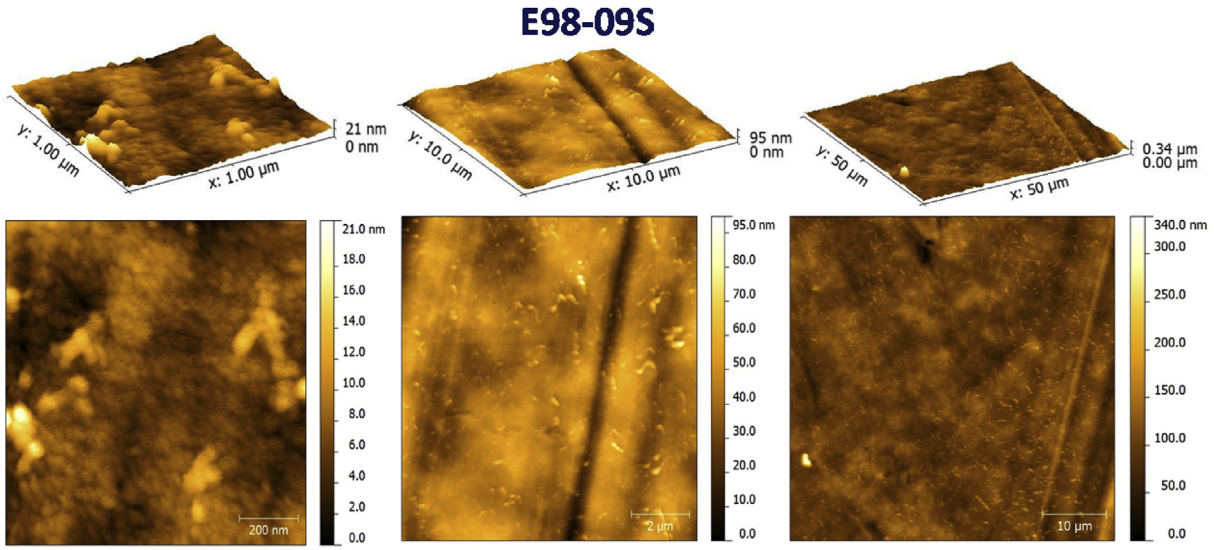

Fig. 11. AFM studies in the tapping mode of the extruded (E98-09S) membrane surface: 3D (upper) and 2D (bottom) topography.

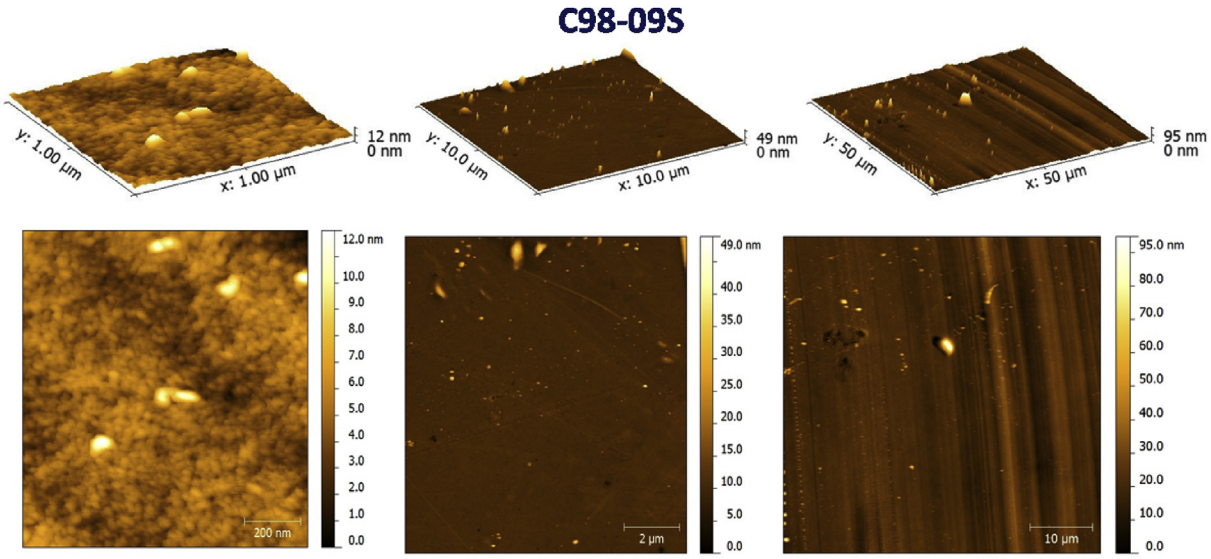

Fig. 12. AFM studies in the tapping mode of the casted (E98-09S) membrane surface: 3D (upper) and 2D (bottom) topography.

Table 4
Roughness properties of extruded and recast membranes derived from the AFM analysis.

Membrane	Dimensions of the analysed area	Roughness analysis mean value R_a/nm
E98-09S	1 µm × 1 µm	1.48
E98-09S	10 µm × 10 µm	8.12
E98-09S	50 µm × 50 µm	13.70
C98-09S side A	1 µm × 1 µm	0.48
C98-09S side A	10 µm × 10 µm	0.57
C98-09S side A	50 µm × 50 µm	10.00
C98-09S side B[a]	1 µm × 1 µm	0.61
C98-09S side B[a]	10 µm × 10 µm	1.66
C98-09S side B[a]	50 µm × 50 µm	2.96

[a] Side B is the part of the casted membrane that was in contact with the glass substrate during the casting procedure.

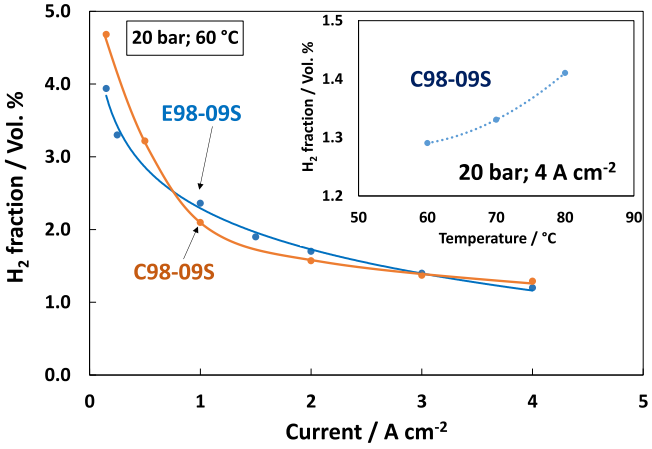

Fig. 13. Hydrogen concentration in the O_2 stream at the anode as function of current density under a 20 bar differential pressure (pressurised H_2, non-pressurised O_2). The inset shows the variation of the H_2 concentration in the O_2 stream of MEA containing recast membrane in the range of temperatures 60–80 °C at 4 A cm^{-2} with a 20 bar differential pressure.

hydrogen production rate [28]. Such phenomenon is a consequence of the occurrence of mass transport limitations within the catalyst-ionomer film [28].

The observed hydrogen cross-over values are similar to those recorded for thicker PFSA membranes under similar operating conditions [28]. These low gas cross-over characteristics combined to the proper voltage efficiency and suitable electrochemical stability at high current density, observed especially for the recast Aquivion® membrane, suggest that this approach can be promising for reliable high current density operation at high differential pressure of electrolysis cells.

Oxygen crossover through the two membranes at ambient pressure was also measured at 60 °C according to a method reported in the literature [65]. Oxygen permeation was significantly lower than hydrogen crossover and comparable for both membranes ($2.1 \pm 0.2 \cdot 10^{-13}$ and $2.3 \pm 0.2 \cdot 10^{-13}$ mol cm^{-1} s^{-1} KPa^{-1} for E98-09S and C98-09S, respectively). The levels of oxygen permeation through the membrane could be even lower when a differential pressure is applied (pressurised hydrogen, non pressurised oxygen). Oxygen pressurisation (balanced pressure) is avoided in the present experiments to reduce oxidation of titanium plates/foams, which is relevant under pressurised oxygen especially when the cell temperature is increased, and to reduce the risk of safety issues.

4. Conclusions

Extruded and recast short-side chain proton exchange Aquivion® membranes have been assessed in membrane-electrode assemblies with regard to their operation at high current density in water electrolysis cells. The membranes were characterised by proper mechanical strength for high-pressure operation and good conductivity to minimise ohmic losses at high current densities. Both membranes have shown a similar voltage efficiency (> 80%) at temperatures of 80–90 °C and high current density (3–4 A cm^{-2}); whereas, the recast membrane was slightly better performing in the activation region of the polarisation curves. At low temperatures, at practical operating conditions (1.8 V), the recast membrane showed lower series resistance but slightly higher polarisation resistance than the extruded membrane under electrolysis conditions. The membrane thickness of 90 µm was appropriate to minimise hydrogen concentration in the oxygen stream at suitable differential pressure during operation and practical current densities (1–4 A cm^{-2}). Hydrogen permeation studies at a differential pressure of 20 bar showed low concentration of H_2 in the oxygen stream for both membranes (< 2%) at 1–4 A cm^{-2} and proper faradaic efficiency > 99%. Different swelling properties and morphological characteristics of the extruded and recast membrane surfaces could have caused different interaction with the catalytic layers. This appeared to have an influence

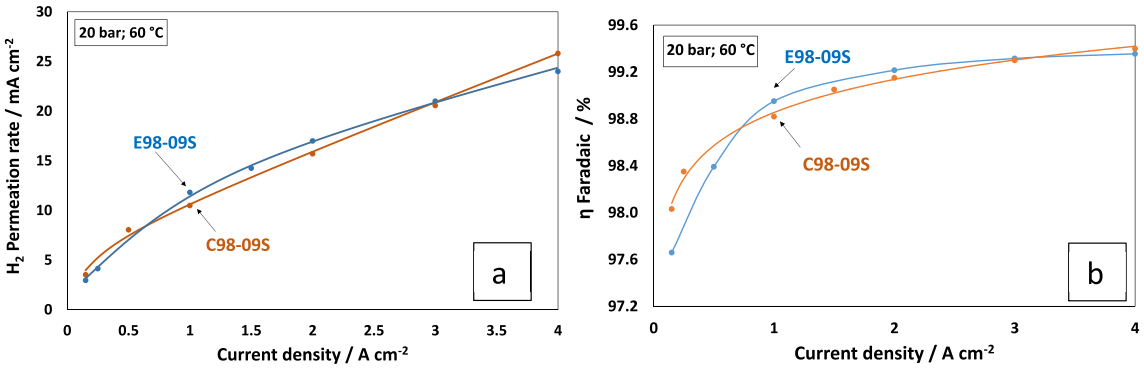

Fig. 14. (a) Equivalent current density for the hydrogen permeation to the anode and (b) Faradaic efficiency as function of electrolysis current density for the extruded E98-09S and cast C98-09S membrane containing MEAs at 20 bar differential pressure and 60 °C.

on the occurrence of recoverable losses during durability studies at high current density with the recast membrane showing better stability.

Declarations of interest

Extruded Aquivion® membranes are sold by Solvay Specialty Polymers.

Acknowledgements

The financial support from the NEPTUNE EU FCH JU project is acknowledged. This project has received funding from Fuel Cells and Hydrogen 2 Joint Undertaking under grant agreement N° 779540. This Joint Undertaking receives support from the European Union's Horizon 2020 research and innovation programme and Hydrogen Europe and Hydrogen Europe Research.

CO and ST would like to thank L. Molteni and G. Salvatore (Solvay Specialty Polymers) for in-plane conductivity measurements and stress-strain tests, respectively.

MAN and LM would like to thank F. A. Scaramuzzo (Sapienza University of Rome) for AFM measurements, performed at CNIS research center of Sapienza University of Rome, and useful discussion.

Appendix A. Supplementary data

Supplementary data to this article can be found online at https://doi.org/10.1016/j.memsci.2019.02.021.

References

[1] F. Barbir, PEM electrolysis for production of hydrogen from renewable energy sources, Sol. Energy 78 (2005) 661–669, https://doi.org/10.1016/j.solener.2004.09.003.

[2] M. Wang, Z. Wang, X. Gong, Z. Guo, The intensification technologies to water electrolysis for hydrogen production - a review, Renew. Sustain. Energy Rev. 29 (2014) 573–588, https://doi.org/10.1016/j.rser.2013.08.090.

[3] P. Millet, N. Mbemba, S.A. Grigoriev, V.N. Fateev, A. Aukauloo, C. Etiévant, Electrochemical performances of PEM water electrolysis cells and perspectives, Int. J. Hydrog. Energy 36 (2011) 4134–4142, https://doi.org/10.1016/j.ijhydene.2010.06.105.

[4] D. Aili, M.K. Hansen, J.W. Andreasen, J. Zhang, J.O. Jensen, N.J. Bjerrum, Q. Li, Porous poly(perfluorosulfonic acid) membranes for alkaline water electrolysis, J. Membr. Sci. 493 (2015) 589–598, https://doi.org/10.1016/j.memsci.2015.06.057.

[5] S. Chu, Y. Cui, N. Liu, The path towards sustainable energy, Nat. Mater. 16 (2017) 16–22, https://doi.org/10.1038/nmat4834.

[6] E. Rasten, G. Hagen, R. Tunold, Electrocatalysis in water electrolysis with solid polymer electrolyte, Electrochim. Acta 48 (2003) 3945–3952, https://doi.org/10.1016/j.electacta.2003.04.001.

[7] M. Balat, Potential importance of hydrogen as a future solution to environmental and transportation problems, Int. J. Hydrog. Energy 33 (2008) 4013–4029, https://doi.org/10.1016/j.ijhydene.2008.05.047.

[8] M. Carmo, D.L. Fritz, J. Mergel, D. Stolten, A comprehensive review on PEM water electrolysis, Int. J. Hydrog. Energy 38 (2013) 4901–4934, https://doi.org/10.1016/j.ijhydene.2013.01.151 19.

[9] A.S. Aricò, S. Siracusano, N. Briguglio, V. Baglio, A. Di Blasi, V. Antonucci, Polymer electrolyte membrane water electrolysis: status of technologies and potential applications in combination with renewable power sources, J. Appl. Electrochem. 43 (2013) 107–118, https://doi.org/10.1007/s10800-012-0490-5.

[10] S.A. Grigoriev, V.I. Porembskiy, S.V. Korobtsev, V.N. Fateev, F. Auprêtre, P. Millet, High-pressure, PEM water electrolysis and corresponding safety issues, Int. J. Hydrog. Energy 36 (2011) 2721–2728 https://doi.org/10.1016/j.ijhydene.2010.03.058.

[11] H. Janssen, J.C. Bringmann, B. Emonts, Safety-related studies on hydrogen production in high-pressure electrolysers, Int. J. Hydrog. Energy 29 (2004) 759–770 https://doi.org/10.1016/j.ijhydene.2003.08.014.

[12] B. Bensmann, R. Hanke-Rauschenbach, I.K. Peña Arias, K. Sundmacher, Energetic evaluation of high pressure PEM electrolyzer systems for intermediate storage of renewable energies, Electrochim. Acta 110 (2013) 570–580 https://doi.org/10.1016/j.electacta.2013.05.102.

[13] M. Schalenbach, M. Carmo, D.L. Fritz, J. Mergel, D. Stolten, Pressurized, PEM water electrolysis: efficiency and gas crossover, Int. J. Hydrog. Energy 38 (2013) 14921–14933 https://doi.org/10.1016/j.ijhydene.2013.09.013.

[14] M. Schalenbach, A.R. Zeradjanin, O. Kasian, S. Cherevko, K.J.J. Mayrhofer, A perspective on low-temperature water electrolysis - challenges in alkaline and acidic technology, Int. J. Electrochem. Sci. 13 (2018) 1173–1226, https://doi.org/10.20964/2018.02.26.

[15] A. Hussain, S.M. Arif, M. Aslam, Emerging renewable and sustainable energy technologies: state of the art, Renew. Sustain. Energy Rev. 71 (2017) 12–28, https://doi.org/10.1016/j.rser.2016.12.033.

[16] I. Hadjipaschalis, A. Poullikkas, V. Efthimiou, Overview of current and future energy storage technologies for electric power applications, Renew. Sustain. Energy Rev. 13 (2009) 1513–1522, https://doi.org/10.20964/2018.02.26.

[17] M. Bernt, H. Gasteiger, A. Influence of ionomer content in IrO_2/TiO_2 electrodes on PEM water electrolyzer performance, J. Electrochem. Soc. 163 (2016) F3179–F3189, https://doi.org/10.1149/2.0231611jes.

[18] S. Siracusano, V. Baglio, N. Van Dijk, L. Merlo, A.S. Aricò, Enhanced performance and durability of low catalyst loading PEM water electrolyser based on a short-side chain perfluorosulfonic ionomer, Appl. Energy 192 (2017) 477–489, https://doi.org/10.1016/j.apenergy.2016.09.011.

[19] S. Siracusano, N. Hodnik, P. Jovanovic, F. Ruiz-Zepeda, M. Šala, V. Baglio, A.S. Aricò, New insights into the stability of a high performance nanostructured catalyst for sustainable water electrolysis, Nano Energy 40 (2017) 618–632, https://doi.org/10.1016/j.nanoen.2017.09.014.

[20] S. Siracusano, S. Trocino, N. Briguglio, V. Baglio and A. S. Aricò, Electrochemical impedance spectroscopy as a diagnostic tool in polymer electrolyte membrane electrolysis, Materials, 11 (8) 1368. DOI: 10.3390/ma11081368.

[21] K. Elsøe, L. Grahl-Madsen, G.G. Scherer, J. Hjelm, M.B. Mogensen, Electrochemical characterization of a PEMEC using impedance spectroscopy, J. Electrochem. Soc. 164 (2017) F1419–F1426, https://doi.org/10.1149/2.0651713jes.

[22] J.B. Ballengee, P.N. Pintauro, Preparation of nanofiber composite proton-exchange membranes from dual fiber electrospun mats, J. Membr. Sci. 442 (2013) 187–195 https://doi.org/10.1016/j.memsci.2013.04.023.

[23] P. Xiao, J.S. Li, H.L. Tang, Z. Wang, M. Pan, Physically stable and high performance Aquivion/ePTFE composite membrane for high temperature fuel cell application, J. Membr. Sci. 442 (2013) 65–71 https://doi.org/10.1016/j.memsci.2013.04.014.

[24] R. Sood, S. Cavaliere, D.J. Jones, J. Rozière, Electrospun nanofibre composite polymer electrolyte fuel cell and electrolysis membranes, Nano Energy 26 (2016) 729–745 https://doi.org/10.1016/j.nanoen.2016.06.027.

[25] S. Shi, A.Z. Weber, A. Kusoglu, Structure/property relationship of Nafion XL composite membranes, J. Membr. Sci. 516 (2016) 123–134 https://doi.org/10.1016/j.memsci.2016.06.004.

[26] V. Schröder, B. Emonts, H. Janßen, H.-P. Schulze, Explosion limits of hydrogen/oxygen mixtures at initial pressures up to 200 bar, Chem. Eng. Technol. 27 (2004) 847–851, https://doi.org/10.1002/ceat.200403174.

[27] S.A. Grigoriev, P. Millet, S.V. Korobtsev, V.I. Porembskiy, M. Pepic, C. Etievant, C. Puyenchet, V.N. Fateev, Hydrogen safety aspects related to high-pressure polymer electrolyte membrane water electrolysis, Int. J. Hydrog. Energy 34 (2009) 5986–5991, https://doi.org/10.1016/j.ijhydene.2009.01.047.

[28] P. Trinke, B. Bensmann, R. Hanke-Rauschenbach, Current density effect on

hydrogen permeation in PEM water electrolyzers, Int. J. Hydrog. Energy 42 (2017) 14355–14366, https://doi.org/10.1016/j.ijhydene.2017.03.231.
[29] H. Ito, N. Miyazaki, M. Ishida, A. Nakano, Cross-permeation and consumption of hydrogen during proton exchange membrane electrolysis, Int. J. Hydrog. Energy 41 (2016) 20439–20446, https://doi.org/10.1016/j.ijhydene.2016.08.119.
[30] D. Bessarabov, A.J. Kruger, S.M. Luopa, J. Park, A.A. Molnar, K.A. Lewinski, Gas crossover mitigation in PEM water electrolysis: hydrogen cross-over benchmark study of 3M's Ir-NSTF based electrolysis catalyst-coated membranes, ECS Trans. 75 (2016) 1165–1173, https://doi.org/10.1149/07514.1165ecst.
[31] S. Abdalla, F. Al-Marzouki, A. Obaid, Safety considerations during production and consumption of hydrogen using proton exchange membrane electrolysis, J. Renew. Sustain. Energy 9 (2017) 013101, , https://doi.org/10.1063/1.4973859 DOI: 10.1149/2.0541807jes.
[32] P. Trinke, P. Haug, J. Brauns, B. Bensmann, R. Hanke-Rauschenbach, T. Turek, Hydrogen crossover in PEM and alkaline water electrolysis: mechanisms, direct comparison and mitigation strategies, J. Electrochem. Soc. 165 (2018) F502–F513, https://doi.org/10.1149/2.0541807jes.
[33] A. Ghielmi, P. Vaccarono, C. Troglia, V. Arcella, Proton exchange membranes based on the short-side-chain perfluorinated ionomer, J. Power Sources 145 (2005) 108–115 https://doi.org/10.1016/j.jpowsour.2004.12.068.
[34] A.S. Aricò, V. Baglio, A. Di Blasi, V. Antonucci, L. Cirillo, A. Ghielmi, V. Arcella, Proton exchange membranes based on the short-side-chain perfluorinated ionomer for high temperature direct methanol fuel cells, Desalination 199 (2006) 271–273, https://doi.org/10.1016/j.desal.2006.03.069.
[35] A.S. Aricò, A. Di Blasi, G. Brunaccini, F. Sergi, G. Dispenza, L. Andaloro, M. Ferraro, V. Antonucci, P. Asher, S. Buche, D. Fongalland, G.A. Hards, J.D.B. Sharman, A. Bayer, G. Heinz, N. Zandonà, R. Zuber, M. Gebert, M. Corasaniti, A. Ghielmi, D.J. Jones, High temperature operation of a solid polymer electrolyte fuel cell stack based on a new ionomer membrane, Fuel Cells 10 (2010) 1013–1023 https://doi.org/10.1002/fuce.201000031.
[36] A. Stassi, I. Gatto, E. Passalacqua, V. Antonucci, A.S. Arico, L. Merlo, C. Oldani, E. Pagano, Performance comparison of long and short-side chain perfluorosulfonic membranes for high temperature polymer electrolyte membrane fuel cell operation, J. Power Sources 196 (2011) 8925–8930, https://doi.org/10.1016/j.jpowsour.2010.12.084.
[37] J. Li, M. Pan, H. Tang, Understanding short-side-chain perfluorinated sulfonic acid and its application for high temperature polymer electrolyte membrane fuel cells, RSC Adv. 4 (2014) 3944–3965 https://doi.org/10.1039/c3ra43735c.
[38] M. Casciola, P. Cojocaru, A. Donnadio, S. Giancola, L. Merlo, Y. Nedellec, M. Pica, S. Subianto, Zirconium phosphate reinforced short side chain perflurosulfonic acid membranes for medium temperature proton exchange membrane fuel cell application, J. Power Sources 262 (2014) 407–413 https://doi.org/10.1016/j.jpowsour.2014.04.010.
[39] C. Boaretti, L. Pasquini, R. Sood, S. Giancola, A. Donnadio, M. Roso, M. Modesti, S. Cavaliere, Mechanically stable nanofibrous sPEEK/Aquivion® composite membranes for fuel cell applications, J. Membr. Sci. 545 (2018) 66–74 https://doi.org/10.1016/j.memsci.2017.09.055.
[40] X. Wu, R. Scott, V. Puthiyapura, Polymer electrolyte membrane water electrolyser with Aquivion® short side chain perfluorosulfonic acid ionomer binder in catalyst layers, Int. J. Hydrog. Energy 37 (18) (2012) 13243–13248, https://doi.org/10.1016/j.ijhydene.2012.06.093.
[41] A.S. Aricò, Electrohypem Project Presentation at the FCH JU Programme Review Days, (2012) http://www.fchju.eu/sites/default/files/ELECTROHYPEM_FCH_Review_Day%202012.pdf.
[42] A. Skulimowska, M. Dupont, M. Zatoń, S. Sunde, L. Merlo, D.J. Jones, J. Rozière, Proton exchange membrane water electrolysis with short-side-chain Aquivion® membrane and IrO2 anode catalyst, Int. J. Hydrog. Energy 39 (2014) 6307–6316 https://doi.org/10.1016/j.ijhydene.2014.02.082.
[43] S. Siracusano, V. Baglio, A. Stassi, L. Merlo, E. Moukheiber, A.S. Arico, Performance analysis of short-side-chain Aquivion® perfluorosulfonic acid polymer for proton exchange membrane water electrolysis, J. Membr. Sci. 466 (2014) 1–7 https://doi.org/10.1016/j.memsci.2014.04.030.
[44] S. Siracusano, V. Baglio, E. Moukheiber, L. Merlo, A.S. Aricò, Performance of a PEM water electrolyser combining an IrRu-oxide anode electrocatalyst and a shortside chain Aquivion membrane, Int. J. Hydrog. Energy 40 (2015) 14430–14435, https://doi.org/10.1016/j.ijhydene.2015.04.159.
[45] S. Giancola, M. Zatoń, Á. Reyes-Carmona, M. Dupont, A. Donnadio, S. Cavaliere, J. Rozière, D.J. Jones, Composite short side chain PFSA membranes for PEM water electrolysis, J. Membr. Sci. 570–571 (2019) 69–76, https://doi.org/10.1016/j.memsci.2018.09.063.
[46] S. Cherevko, S. Geiger, O. Kasian, N. Kulyk, J.-P. Grote, A. Savan, B.R. Shrestha, S. Merzlikin, B. Breitbach, A. Ludwig, K.J. Mayrhofer, Catal. Today 262 (2015) 170–180, https://doi.org/10.1016/j.cattod.2015.08.014.
[47] H. Yu, N. Danilovic, Y. Wang, W. Willis, A. Poozhikunnath, L. Bonville, C. Capuano, K. Ayers, R. Maric, Nano-size IrOx catalyst of high activity and stability in PEM water electrolyzer with ultra-low iridium loading, Appl. Catal. B Environ. 239 (2018) 133–146, https://doi.org/10.1016/j.apcatb.2018.07.064.
[48] P. Lettenmeier, R. Wang, R. Abouatallah, S. Helmly, T. Morawietz, R. Hiesgen, S. Kolb, F. Burggraf, J. Kallo, A.S. Gago, K.A. Friedrich, Durable membrane electrode assemblies for proton exchange membrane electrolyzer systems operating at high current densities, Electrochim. Acta 210 (2016) 502–511, https://doi.org/10.1016/j.electacta.2016.04.164.
[49] M.-H. Kim, C.J. Glinka, S.A. Grot, W.G. Grot, SANS study of the effects of water vapor sorption on the nanoscale structure of perfluorinated sulfonic acid (NAFION) membranes, Macromolecules 39 (2006) 4775–4787, https://doi.org/10.1021/ma060576u.
[50] V. Antonucci, A. Di Blasi, V. Baglio, R. Ornelas, F. Matteucci, J. Ledesma-Garcia, L.G. Arriaga, A.S. Aricò, High temperature operation of a composite membrane based solid polymer electrolyte water electrolyser, Electrochim. Acta 53 (2008) 7350–7356 https://doi.org/10.1016/j.electacta.2008.04.009.
[51] D. Zhang, K. Zeng, Evaluating the behavior of electrolytic gas bubbles and their effect on the cell voltage in alkaline water electrolysis, Ind. Eng. Chem. Res. 51 (2012) 13825–13832, https://doi.org/10.1021/ie301029e.
[52] S. Giddey, F.T. Ciacchi, S.P.S. Badwal, High purity oxygen production with a polymer electrolyte membrane electrolyser, J. Membr. Sci. 346 (1) (2010) 227–232, https://doi.org/10.1016/j.memsci.2009.09.042.
[53] P.J. James, M. Antognozzi, J. Tamayo, T.J. McMaster, J.M. Newton, M.J. Miles, Interpretation of contrast in tapping mode AFM and shear force microscopy. A study of nafion, Langmuir 17 (2001) 349–360, https://doi.org/10.1021/la000332h.
[54] S.F. Timashev, D.G. Bessarabov, R.D. Sanderson, S. Marais, S.G. Lakeev, Description of non-regular membrane structures: a novel phenomenological approach, J. Membr. Sci. 170 (2000) 191–203, https://doi.org/10.1016/S0376-7388(99)00367-1.
[55] R. Hiesgen, T. Morawietz, M. Handl, M. Corasaniti, K.A. Friedrich, Atomic force microscopy on cross sections of fuel cell membranes, electrodes, and membrane electrode assemblies, Electrochim. Acta 162 (2015) 86–99 https://doi.org/10.1016/j.electacta.2014.11.122.
[56] R. Hiesgen, T. Morawietz, M. Handl, M. Corasaniti, K.A. Friedrich, Insight into the structure and nanoscale conductivity of fluorinated ionomer membranes, J. Electrochem. Soc. 161 (12) (2014) F1214–F1223, https://doi.org/10.1149/2.0701412jes.
[57] A.H. Reksten, H. Thuv, F. Seland, S. Sunde, The oxygen evolution reaction mechanism at IrxRu1 − xO2 powders produced by hydrolysis synthesis, J. Electroanal. Chem. 819 (2018) 547–561, https://doi.org/10.1016/j.jelechem.2018.04.018.
[58] B. Bensmann, R. Hanke-Rauschenbach, K. Sundmacher, In-situ measurement of hydrogen crossover in polymer electrolyte membrane water electrolysis, Int. J. Hydrog. Energy 39 (2014) 49–53 https://doi.org/10.1016/j.ijhydene.2013.10.085.
[59] P. Trinke, B. Bensmann, S. Reichstein, R. Hanke-Rauschenbach, K. Sundmacher, Impact of pressure and temperature on hydrogen permeation in PEM water electrolyzers operated at asymmetric pressure conditions, ECS Trans. 75 (14) (2016) 1081–1094, https://doi.org/10.1149/07514.1081ecst.
[60] P. Trinke, B. Bensmann, S. Reichstein, R. Hanke-Rauschenbach, K. Sundmacher, Hydrogen permeation in PEM electrolyzer cells operated at asymmetric pressure conditions, J. Electrochem. Soc. 163 (11) (2016) F3164–F3170, https://doi.org/10.1149/2.0221611jes.
[61] N. Briguglio, S. Siracusano, G. Bonura, D. Sebastián, A.S. Aricò, Flammability reduction in a pressurised water electrolyser based on a thin polymer electrolyte membrane through a Pt-alloy catalytic approach, Appl. Catal. B Environ. 246 (2019) 254–265, https://doi.org/10.1016/j.apcatb.2018.12.079.
[62] V. Schröder, B. Emonts, H. Janßen, H.-P. Schulze, Explosion limits of hydrogen/oxygen mixtures at initial pressures up to 200 bar, Chem. Eng. Technol. 27 (8) (2004) 847–851, https://doi.org/10.1002/ceat.200403174.
[63] H. Janssen, J.C. Bringmann, B. Emonts, V. Schroeder, Safety-related studies on hydrogen production in high-pressure electrolysers, Int. J. Hydrog. Energy 29 (7) (2004) 759–770, https://doi.org/10.1016/j.ijhydene.2003.08.014.
[64] S. Hink, D. Henkensmeier, J.H. Jang, H.-J. Kim, J. Han, S.-W. Nam, Reduced in-plane swelling of Nafion by a biaxial modification process, Macromol. Chem. Phys. 216 (11) (2015) 1235–1243, https://doi.org/10.1002/macp.201500063.
[65] J. Zhang, H.A. Gasteiger, W. Gu, Electrochemical measurement of the oxygen permeation rate through polymer electrolyte membranes, J. Electrochem. Soc. 160 (6) (2013) F616–F622, https://doi.org/10.1149/2.081306jes.